

# Free-carrier induced nonlinear dynamics in hybrid graphene-based photonic waveguides

Ambaresh Sahoo,<sup>1, 2</sup> Andrea Marini,<sup>3</sup> and Samudra Roy<sup>1, \*</sup>

<sup>1</sup>*Department of Physics, Indian Institute of Technology Kharagpur, West Bengal 721302, India*

<sup>2</sup>*Department of Physics, Indian Institute of Technology Guwahati, Assam 781039, India*

<sup>3</sup>*Department of Physical and Chemical Sciences,  
University of L'Aquila, Via Vetoio, 67100 L'Aquila, Italy*

We develop from first principles a theoretical model for infrared pulse propagation in graphene-covered hybrid waveguides. We model electron dynamics in graphene by Bloch equations, enabling the derivation of the nonlinear conductivity and of a rate equation accounting for free-carrier generation. Radiation propagation is modeled through a generalized nonlinear Schrödinger equation for the field envelope coupled with the rate equation accounting for the generation of free carriers in graphene. Our numerical simulations clearly indicate that unperturbed Kerr solitons accelerate due to the carrier-induced index change and experience a strong self-induced spectral blue-shift. Our numerical results are fully explained by semi-analytical predictions based on soliton perturbation theory.

## I. INTRODUCTION

Optical nonlinearity plays a key role in several modern and future photonic applications. In particular, nonlinear ultrafast effects at the femtosecond timescale are promising for optical information processing with petahertz bandwidth exceeding the speed of current electronic devices by six orders of magnitude [1, 2]. Guided waves in integrated nonlinear optical devices offer the fundamental advantage of radiation confinement leading to high field intensity that can be exploited over propagation [3]. Silicon photonics is promising for a plethora of integrated optical devices [4], but the nonlinear optical functionalities of silicon are inherently limited by two-photon absorption [5–7]. Plasmonic waveguides offer an alternative platform for integrated nonlinear optical processing [8, 9] thanks to the inherently high nonlinearity of metals [10–15] that is further enhanced by the surface confinement [16–18]. However, the high ohmic losses of metals pose a stringent limitation for the development of nonlinear plasmonic circuits [19]. Absorption mitigation strategies in plasmonic devices resort to amplification schemes [20–26], surface roughness reduction [27], and self-induced transparency plasmon soliton excitation [28].

Graphene offers an appealing alternative to metals for integrated nonlinear optical applications [29] thanks to ultra-high electron mobility [30, 31] and its peculiar conical band structure [32], which inherent anharmonicity leads to large nonlinear optical interaction [33–38] that can be exploited, e.g., for high-harmonic generation [39, 40] and many other nonlinear optical applications [41]. Furthermore, the ultrafast nonlinear dynamics of Massless Dirac Fermions (MDFs) in graphene involve the photo-generation of free-carriers (FCs) at the femtosecond timescale [42], which has already been employed for self-phase modulation in integrated nonlinear wave-

guides embedding graphene [43, 44] and is promising for a plethora of future integrated optoelectronic applications.

Here, we investigate the ultrafast nonlinear dynamics of intense infrared radiation pulses propagating in a photonic waveguide covered by graphene, unveiling the role played by FCs in the spectral modulation observed. Within the MDF framework governing graphene infrared response, we derive a Generalized Nonlinear Schrödinger Equation (GNLSE) accounting for graphene Kerr nonlinearity, saturable absorption and ultrafast dynamics of the photo-generated FCs. We further investigate soliton dynamics through a semi-analytical technique based on Lagrange's variational method to theoretically capture the effect produced by FCs, deriving a set of ordinary differential equations describing the evolution of soliton parameters [45, 46]. Our calculations reveal that photo-generated FCs produce a peculiar signature in the temporal dynamics of optical solitons that undergo a substantial spectral blueshift accompanied by a temporal acceleration over propagation. Such a blueshift arises from the pulse self-action through a self-induced asymmetric refractive index temporal modulation produced by the photo-generated FCs. Our analytical predictions are confirmed by direct numerical simulations of the GNLSE, and indicate that photonic waveguides covered by graphene offer a promising platform for integrated spectral modulation of infrared radiation.

## II. THEORETICAL FRAMEWORK

In order to describe nonlinear ultrafast dynamics of infrared radiation pulses in hybrid graphene-covered waveguides, we consider a realistic design for a TaFD5 glass square waveguide covered by undoped graphene on top, deposited over a silica glass substrate and surrounded by air, as schematically depicted in Fig. 1(a), which can be practically realized with existing state-of-art fabrication techniques. A single layer of graphene is

\* samudra.roy@phy.iitkgp.ac.in

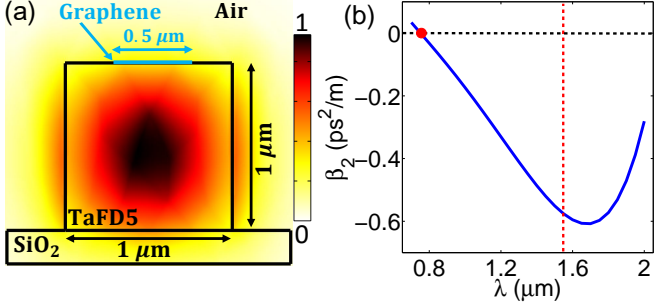


FIG. 1. (Color online) (a) A TaFD5 glass waveguide with core dimensions (height  $\times$  width)  $1\mu\text{m} \times 1\mu\text{m}$  covered by a single layer of graphene on top. The electric field intensity distribution  $|\mathbf{e}(x, y)|^2$  of the fundamental quasi-TE mode at  $\lambda_0 = 1.55\ \mu\text{m}$  is depicted in the inset in dimensionless units. (b) Group velocity dispersion profile of the fundamental mode calculated by finite-element frequency-domain calculations [54]. The input ( $\lambda_0 = 1.55\ \mu\text{m}$ ) and zero-dispersion ( $\lambda_{\text{ZD}} \simeq 0.75\ \mu\text{m}$ ) wavelengths are indicated by the vertical dotted red line and the solid red dot, respectively.

deposited on top of the TaFD5 core where, upon infrared excitation, the FCs are accumulated over the propagation distance. The TaFD5 core is Raman-inactive [50, 51] and linear/nonlinear absorption of TaFD5 is negligible over  $\sim \text{cm}$  propagation distances. Hence, TaFD5-based waveguides covered by single-layer graphene enable the full exploitation of photo-excited FCs in the graphene layer to attain efficient spectral modulation of the propagating pulse [52]. Alternatively, one can use silicon nitride ( $\text{Si}_3\text{N}_4$ ) as a core material with similar waveguide structure for the exact same purpose, as it is also Raman-inactive and the linear and nonlinear losses are ultralow at the visible and infrared wavelengths [53]. In Fig. 1(a) we illustrate the cross-section of the waveguide and the intensity distribution of the fundamental quasi-TE mode at  $\lambda_0 = 1.55\ \mu\text{m}$  that we calculate numerically by finite element simulations [54]. We further calculate numerically the group-velocity dispersion (GVD) of the waveguide quasi-TE mode in the  $0.7\text{--}2.0\ \mu\text{m}$  wavelength range, which is indicated in Fig. 1(b) by the solid blue line.

### A. Electron dynamics in graphene

To investigate the nonlinear spatio-temporal dynamics of infrared pulses in the proposed hybrid waveguide, we consider a pulse with electric field  $\mathcal{E}(\mathbf{r}, t) = \text{Re}[u(z, t)\mathbf{e}(x, y)e^{i\beta_0 z - i\omega_0 t}/\sqrt{P}]$ , where  $u(z, t)$  is the pulse envelope,  $\mathbf{e}(x, y)$  and  $P$  are the quasi-TE mode profile and scaling modal power calculated numerically,  $\beta_0 \simeq 6.2967 \times 10^6\ \text{rad/m}$  is the carrier wave-vector and  $\omega_0 = 2\pi c/\lambda_0 \simeq 1.216 \times 10^{15}\ \text{rad/sec}$  is the carrier frequency. We emphasize that, in the considered geometry, the electric field profile of the quasi-TE mode  $\mathbf{e}(x, y_0) \simeq e_0 \hat{\mathbf{x}}$  is practically uniform (independent of  $x$ ) over the graphene layer at  $y_0 = 1\ \mu\text{m}$ , see Fig. 1(a), and directed over the  $x$ -

direction. In turn, we approximate the electric field over the graphene flake as  $\mathbf{E}(z, t) = \text{Re}[\mathbf{E}_0(z, t)e^{i\beta_0 z - i\omega_0 t}]$ , where  $\mathbf{E}_0(z, t) = u(z, t)e_0 \hat{\mathbf{x}}/\sqrt{P}$ , which corresponds to the vector potential  $\mathbf{A}(z, t) = -\int_{-\infty}^t \mathbf{E}(z, t') dt'$ . In the MDF picture, the two-component spinor  $\psi_{\mathbf{k}}$  of a single electron in graphene with initial in-plane wave-vector  $\mathbf{k}$  satisfies the single-particle time-dependent Dirac equation

$$i\hbar \partial_t \psi_{\mathbf{k}}(z, t) = \hat{H}_{\mathbf{k}}(z, t) \psi_{\mathbf{k}}(z, t), \quad (1)$$

with spatiotemporal-dependent Hamiltonian  $\hat{H}_{\mathbf{k}}(z, t) = v_{\text{F}} \boldsymbol{\pi} \cdot \boldsymbol{\sigma}$ , where  $v_{\text{F}} \simeq c/300$  is the Fermi velocity,  $\boldsymbol{\pi}(z, t) = \hbar \mathbf{k} + e \mathbf{A}(z, t)$  is the electron quasi-momentum with  $-e$  being the electron charge and  $\boldsymbol{\sigma} = (\sigma_x, \sigma_y)$  the two-dimensional Pauli-matrix vector. We emphasize that, owing to the conical band-structure of graphene, infrared excitation is resonant at  $k_{\text{res}} = \omega_0/2v_{\text{F}} \simeq 6.1 \times 10^8\ \text{rad/m}$  and in turn  $\beta_0 \ll k_{\text{res}}$ . Therefore, we remark that the  $z$ -dependence of the Hamiltonian  $\hat{H}_{\mathbf{k}}(z, t)$  is intended as adiabatic. Introducing the spatiotemporal-dependent energy  $\varepsilon_{\mathbf{k}}(z, t) = v_{\text{F}} |\boldsymbol{\pi}(z, t)|$  one can express the Hamiltonian above as

$$\hat{H}_{\mathbf{k}}(z, t) = \varepsilon_{\mathbf{k}}(z, t) \begin{pmatrix} 0 & e^{-i\theta_{\mathbf{k}}(z, t)} \\ e^{i\theta_{\mathbf{k}}(z, t)} & 0 \end{pmatrix}, \quad (2)$$

where  $\theta_{\mathbf{k}}(z, t) = \text{atan}[\pi_y(z, t)/\pi_x(z, t)]$ . Following a previously reported nonperturbative approach [47], we set the spinor Ansatz as a linear combination of upper and lower states  $\psi_{\mathbf{k}}^{\pm}$

$$\psi_{\mathbf{k}}(z, t) = c_{\mathbf{k}}^+(z, t) \psi_{\mathbf{k}}^+(z, t) + c_{\mathbf{k}}^-(z, t) \psi_{\mathbf{k}}^-(z, t), \quad (3)$$

where  $\psi_{\mathbf{k}}^{\pm}(z, t) = (1/\sqrt{2})e^{\mp i\Omega_{\mathbf{k}}(z, t)} [e^{-i\theta_{\mathbf{k}}(z, t)/2}, \pm e^{i\theta_{\mathbf{k}}(z, t)/2}]^T$  and  $\Omega_{\mathbf{k}}(z, t) = (1/\hbar) \int_{-\infty}^t \varepsilon_{\mathbf{k}}(z, t') dt'$  is the instantaneous phase. Inserting the Ansatz given by Eq. (3) into Eq. (1) one gets the temporal evolution of the coefficients  $c_{\mathbf{k}}^{\pm}(z, t)$ ,

$$\dot{c}_{\mathbf{k}}^{\pm}(z, t) = \frac{i}{2} \dot{\theta}_{\mathbf{k}}(z, t) c_{\mathbf{k}}^{\mp}(z, t) \exp[\pm 2i\Omega_{\mathbf{k}}(z, t)]. \quad (4)$$

Introducing the interband coherence  $\rho_{\mathbf{k}} = c_{\mathbf{k}}^+ c_{\mathbf{k}}^{-*}$  and population difference  $n_{\mathbf{k}} = |c_{\mathbf{k}}^+|^2 - |c_{\mathbf{k}}^-|^2$ , one can rewrite the equation for the coefficients in the form of Bloch Equations,

$$\dot{\rho}_{\mathbf{k}} = -\gamma \rho_{\mathbf{k}} - \frac{i}{2} \dot{\theta}_{\mathbf{k}} n_{\mathbf{k}} \exp(2i\Omega_{\mathbf{k}}) \quad (5)$$

$$\dot{n}_{\mathbf{k}} = -\gamma(n_{\mathbf{k}} + 1) - i \dot{\theta}_{\mathbf{k}} \exp(-2i\Omega_{\mathbf{k}}) \rho + \text{c.c.}, \quad (6)$$

where we have introduced the effective recombination rate  $\gamma = (100\text{fs})^{-1}$  accounting for electron-electron and electron-phonon collisions [42]. In turn, the induced single-electron current is given by  $\mathbf{j}_{\mathbf{k}}^e(z, t) = -e \psi_{\mathbf{k}}^{\dagger}(z, t) \nabla \boldsymbol{\pi} H_{\mathbf{k}}(z, t) \psi_{\mathbf{k}}(z, t) + e \psi_{\mathbf{k}}^{-\dagger}(z, t) \nabla \boldsymbol{\pi} H(z, t) \psi_{\mathbf{k}}^-(z, t)$ , and explicitly

$$\begin{aligned} \mathbf{j}_{\mathbf{k},x}^e(z, t) = & -ev_{\text{F}} [(n_{\mathbf{k}}(z, t) + 1) \cos \theta_{\mathbf{k}}(z, t) + \\ & + i \sin \theta_{\mathbf{k}}(z, t) \left\{ \rho_{\mathbf{k}}(z, t) e^{-2i\Omega_{\mathbf{k}}(z, t)} - \text{c.c.} \right\}] \end{aligned} \quad (7)$$

Then, the macroscopic current  $\mathbf{J}(z, t)$  is calculated by integrating over all in-plane electron wave-vectors

$$\mathbf{J}(z, t) = \frac{g_s g_v}{(2\pi)^2} \hat{\mathbf{x}} \int_{-\infty}^{+\infty} dk_x \int_{-\infty}^{+\infty} dk_y j_{\mathbf{k},x}^e(z, t), \quad (8)$$

where  $g_s = g_v = 2$  are the spin/valley degeneracy factors. Because even at high peak intensities of the order of  $\text{TW/cm}^2$   $eA \ll \hbar k_{\text{res}}$ , in Eqs. (7,8) we neglect the optical momentum  $e\mathbf{A}$  with respect to the electron momentum  $\hbar\mathbf{k}$ , obtaining

$$\begin{aligned} \mathbf{J}(z, t) \simeq \text{Re} \left[ \frac{ie^2 v_F}{\pi^2 \omega_0 \hbar} K_{\text{FC}}(z, t) \mathbf{E}_0(z, t) e^{i\beta_0 z - i\omega_0 t} \right] + \\ + \frac{2ev_F}{\pi^2} \hat{\mathbf{x}} \int_0^{\infty} k dk \int_0^{2\pi} d\phi \sin \phi \text{Im} \Gamma_{\mathbf{k}}(z, t), \end{aligned} \quad (9)$$

where  $K_{\text{FC}}(z, t) = (2v_F/\omega) \int_0^{\infty} k dk \int_0^{2\pi} d\phi [n_{\mathbf{k}}(z, t) + 1]$  is the FC linear density,  $\Gamma_{\mathbf{k}}(z, t) = \rho_{\mathbf{k}}(z, t) e^{-2i\Omega_{0,k}t}$ , and  $\Omega_{0,k} = v_F k$ . To unveil the role played by FCs, we first calculate the stationary solution of Eqs. (5,6) in the slowly varying envelope approximation by setting the Ansatz  $\Gamma_{\mathbf{k}} = \Gamma_{\mathbf{k}}^+ e^{i\omega_0 t} + \Gamma_{\mathbf{k}}^- e^{-i\omega_0 t}$  and  $n_{\mathbf{k}} = n_{0,\mathbf{k}}$ , obtaining

$$\mathcal{G}_{\mathbf{k}} = (\Gamma_{\mathbf{k}}^+ - \Gamma_{\mathbf{k}}^{-*})/E_0^* = -ie k_y n_{0,\mathbf{k}} \eta_{\text{U},k} / 2\hbar k^2 \eta_{\text{L},k}, \quad (10a)$$

$$n_{0,\mathbf{k}} = - \left[ 1 + \frac{e^2 k_y^2 (\gamma^2 + 4\Omega_{0,k}^2 + \omega_0^2)}{2\hbar^2 k^4 \eta_{\text{L},k}} |E_0|^2 \right]^{-1}, \quad (10b)$$

$$\eta_{\text{L},k} = [\gamma^2 + (2\Omega_{0,k} + \omega_0)^2][\gamma^2 + (2\Omega_{0,k} - \omega_0)^2], \quad (10c)$$

$$\eta_{\text{U},k} = (\gamma + i\omega_0)[(\gamma^2 + 4\Omega_{0,k}^2 - \omega_0^2) - 2i\gamma\omega_0]. \quad (10d)$$

Thus, inserting the expressions above in Eq. (6) and integrating over the electron wave-vectors both sides of Eq. (6) we obtain a rate equation for the FC density

$$\partial_t K_{\text{FC}}(z, t) = -\gamma K_{\text{FC}}(z, t) + \Upsilon(z, t) |E_0(z, t)|^2, \quad (11)$$

where  $\Upsilon(z, t) = (\pi^2 v_F e^2 / 2\hbar^2 \omega_0^2) / \sqrt{1 + |E_0(z, t)|^2 / E_{\text{sat}}^2}$  and  $E_{\text{sat}} = \sqrt{2I_{\text{S}}/\epsilon_0 c} = 4.92 \times 10^6 \text{ V/m}$  with  $I_{\text{S}}$  being the saturable intensity of graphene. The equation above accounts for the photo-generation of FCs, which affects radiation dynamics in the hybrid waveguide through the induced macroscopic current  $\mathbf{J}(z, t)$  in Eq. (9), which gives explicitly

$$\mathbf{J} = \text{Re} \left\{ \left[ \frac{ie^2 v_F}{\pi^2 \omega_0 \hbar} K_{\text{FC}} + \sigma(|\mathbf{E}_0|^2) \right] \mathbf{E}_0 e^{i\beta_0 z - i\omega_0 t} \right\}, \quad (12)$$

where  $\sigma(|\mathbf{E}_0|^2)$  is the nonlinear conductivity at the carrier frequency  $\omega_0$ , provided by

$$\sigma(|\mathbf{E}_0|^2) = \frac{2iev_F}{\pi^2} \int_0^{\infty} k dk \int_0^{2\pi} d\phi \sin \phi \mathcal{G}_{\mathbf{k}}^* (|E_0|^2). \quad (13)$$

Following the approach indicated in Ref. [55], we solve numerically the above integral for several radiation intensities  $I = (1/2)\epsilon_0 c |E_0|^2$ , finding excellent fitting with

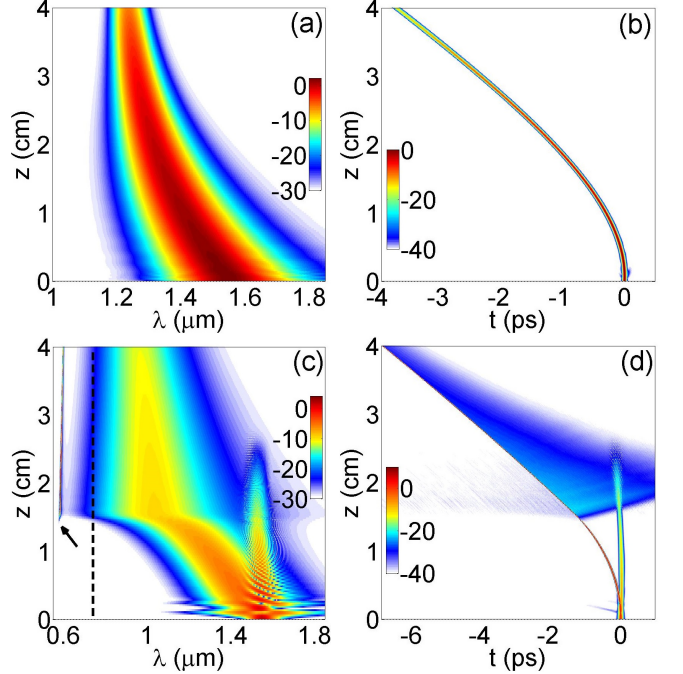


FIG. 2. (Color online) Longitudinal evolution of (a,c) spectral ( $|\tilde{\psi}(\xi, \omega)|^2$ ) and (b,d) temporal ( $|\psi(\xi, \tau)|^2$ ) dynamics of input pulses  $\psi(0, \tau) = \text{sech}(\tau)$  with distinct soliton orders (a,b)  $N = 1$  ( $P_0 = 1.358 \times 10^4 \text{ W}$ ,  $t_0 = 10 \text{ fs}$ ,  $\alpha_0 = 0.316$ ,  $\Theta_{\text{FC}} = 1.0865 \times 10^7$ ,  $\psi_{\text{sat}}^2 = 8.966 \times 10^{-5}$ ) and (c,d)  $N = 2$  ( $P_0 = 8.692 \times 10^3 \text{ W}$ ,  $t_0 = 25 \text{ fs}$ ,  $\alpha_0 = 1.975$ ,  $\Theta_{\text{FC}} = 1.0865 \times 10^8$ ,  $\psi_{\text{sat}}^2 = 1.401 \times 10^{-4}$ ). The vertical dotted line in (c) locates the zero-dispersion wavelength  $\lambda_{\text{ZD}}$  across which resonant radiation (indicated by the arrow) arises due to suppression of FC-mediated self-frequency blueshift [57].

the analytical expression  $\sigma(I)$ :

$$\sigma(I) = \sigma_0 \left[ \frac{1}{\sqrt{1 + I/I_{\text{S}}}} - i \frac{1 - e^{-\eta_1 \sqrt{I/I_{\text{S}}}}}{\sqrt{1 + \eta_2 (I/I_{\text{S}})^{0.4}}} \right],$$

where  $\sigma_0 = e^2 / 4\hbar$ ,  $I_{\text{S}} = 137\hbar\omega_{\text{S}}^2\omega_0^2 / (8\pi v_F^2)$ ,  $\omega_{\text{S}} = 6.16 \text{ rad ps}^{-1}$ ,  $\eta_1 = \omega_{\eta} / \omega_0$ ,  $\eta_2 = (\omega_{\eta} / \omega_0)^{0.8}$ , and  $\omega_{\eta} = 46.20 \text{ rad ps}^{-1}$  [55].

## B. Radiation dynamics in the hybrid waveguide

In order to model radiation dynamics, we assume that nonlinear optical effects are sufficiently weak not to affect the mode structure of the hybrid graphene-covered waveguide. In turn, we calculate the quasi-TE mode profile by finite-element numerical simulations [54] at  $\lambda_0 = 1.55 \mu\text{m}$  neglecting nonlinearity of graphene and the glass core. Note that, for the considered geometry, at  $\lambda_{\text{ZD}} \simeq 0.75 \mu\text{m}$  the GVD coefficient ( $\beta_2$ ) vanishes, see Fig. 1(b), while at the operating wavelength ( $\lambda_0 = 1.55 \mu\text{m}$ )  $\beta_2 \simeq -0.576 \text{ ps}^2/\text{m}$ , the third-order dispersion coefficient is  $\beta_3 \simeq 0.599 \times 10^{-3} \text{ ps}^3/\text{m}$ , and the

Kerr coefficient of TaFD5 is  $\gamma_{\text{TaFD5}} \simeq 0.424 \text{ W}^{-1}\text{m}^{-1}$ . The scaling modal power  $P$  at  $\lambda_0$  is evaluated by the expression  $P = \int_{\text{Full area}} dx dy \text{Re}[\mathbf{e} \times \mathbf{h}^*] \cdot \hat{\mathbf{z}} \simeq 4.434 \times 10^{-12} \text{ W}$ , where  $\mathbf{e}(x, y)$  and  $\mathbf{h}(x, y)$  are the numerically calculated electric and magnetic field profiles of the quasi-TE mode [54]. We further evaluate the average  $x$ -component of the electric field amplitude experienced by the graphene layer at the top midpoint of the TaFD5 surface  $e_0 \simeq (9.178 + i 16.288) \text{ V/m}$ . Note that at  $\lambda_0$  the GVD coefficient is negative  $\beta_2 < 0$ , thus enabling the excitation of bright optical solitons.

Performing an asymptotic expansion of Maxwell's equations, where the nonlinearity of graphene and of the waveguide core are treated as perturbations, following a standard approach detailed in previous works, see, e.g., Ref. [56], we derive a Generalized Nonlinear Schrödinger Equation (GNLSE) for the dimensionless pulse envelope  $\psi(\xi, \tau) = u/\sqrt{P_0}$  in the co-moving reference frame

$$i\partial_\xi\psi + \hat{D}(i\partial_\tau)\psi + N^2(1 + i\tau_{sh}\partial_\tau)|\psi|^2\psi - d_{\text{FC}}\Phi_{\text{FC}}\psi + i\frac{\alpha_0\psi}{\sqrt{1 + 3|\psi|^2/\psi_{\text{sat}}^2}} + \frac{\alpha_0\psi\left(1 - e^{-\eta_1\sqrt{3|\psi|^2/\psi_{\text{sat}}^2}}\right)}{\sqrt{1 + \eta_2(3|\psi|^2/\psi_{\text{sat}}^2)^{0.4}}} = 0, \quad (14)$$

where the dimensionless variable  $\xi = z/L_D$  represents the longitudinal coordinate  $z$  rescaled to the dispersion length  $L_D = t_0^2/|\beta_2|$  and  $\tau = (t - z/v_g)/t_0$  represents the temporal coordinate  $t$  in the co-moving reference frame shifted by  $z/v_g$  and rescaled to the pulse duration  $t_0$ , while  $v_g = 1.5133 \times 10^8 \text{ m/s}$  is the group velocity,  $\alpha_0 = w|e_0|^2\sigma_0 L_D/P$  is the normalized linear absorption rate with  $w$  being the width of the graphene layer,  $L_{\text{NL}} = 1/(\gamma_{\text{TaFD5}} P_0)$  is the nonlinear length with  $P_0$  being the input peak power and  $N^2 = L_D/L_{\text{NL}}$  is the soliton order, and  $\tau_{sh} = 1/\omega_0 t_0$  is the normalized self-steepening coefficient. As anticipated in the previous subsection, the GNLSE is coupled through the coupling coefficient  $d_{\text{FC}} = e^2 v_F w |e_0|^2 / \pi^2 \hbar \omega_0 P = 6.0678 \times 10^{-7}$ , with the rate equation governing the temporal evolution of the normalized FC-density spatio-temporal profile  $\Phi_{\text{FC}}(\xi, \tau) = L_D K_{\text{FC}}(z, t)$ , explicitly given by

$$\frac{\partial \Phi_{\text{FC}}}{\partial \tau} = \frac{\Theta_{\text{FC}}|\psi|^2}{\sqrt{1 + 3|\psi|^2/\psi_{\text{sat}}^2}} - \frac{\Phi_{\text{FC}}}{\tau_{\text{FC}}}, \quad (15)$$

where  $\Theta_{\text{FC}} = L_D t_0 P_0 |e_0|^2 \pi^2 v_F e^2 / (2\hbar^2 P \omega_0^2)$  is the normalized FC generation rate,  $\psi_{\text{sat}}^2 = 3|E_{\text{sat}}/e_0|^2 P/P_0$  is the normalized saturation intensity and  $\tau_{\text{FC}} = 1/\gamma t_0$  is the normalized FC recombination rate arising from electron-electron and electron-phonon collisions.

### III. FC-INDUCED SPECTRAL DYNAMICS

The propagation of infrared radiation pulses with normalized envelope  $\psi$  in the considered graphene-covered hybrid waveguide is governed by Eqs. (14,15) that, as

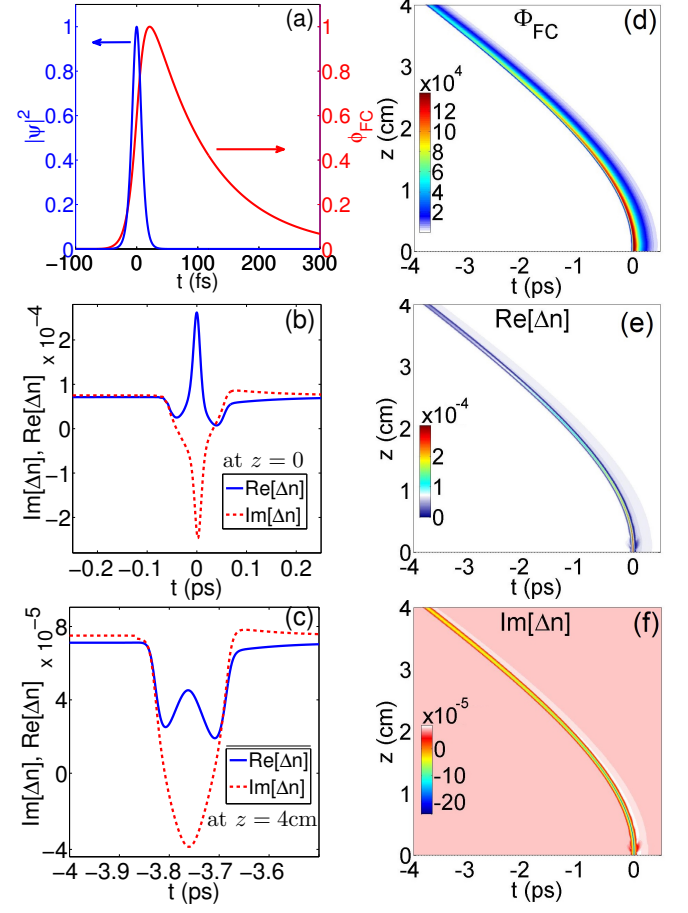


FIG. 3. (Color online) (a) Normalized temporal profile of the FC density  $\Phi_{\text{FC}}(z/L_D, t/t_0)$  (red curve corresponding to the right vertical axis) at  $z = 0$ , and temporal profile of the impinging pulse intensity  $|\psi(0, t/t_0)|^2$  (blue curve corresponding to the left vertical axis) for  $t_0 = 10 \text{ fs}$ . (d) Spatio-temporal evolution of  $\Phi_{\text{FC}}(z/L_D, t/t_0)$ . Real and imaginary parts of the FC-induced refractive index modulation  $\Delta n(z/L_D, t/t_0)$  [see Eq. (16)] at (a) input  $z = 0$  and (b) output  $z = 4 \text{ cm}$ , and their respective spatio-temporal evolutions (e) and (f) for  $N = 1$ .

explained above, account for the nonlinear dynamics produced by the photo-generated FCs in graphene. By adopting the standard split-step fast Fourier transform complemented with fourth-order Runge-Kutta, we solve Eqs. (14,15) numerically considering input pulses in the form of Kerr solitons,  $\psi(0, \tau) = \text{sech}(\tau)$ . In Fig. 2 we illustrate the spectral and temporal evolutions of (a,b) fundamental ( $N = 1$ ) and (c,d) second-order ( $N = 2$ ) solitons. Note that, owing to FC excitation in the graphene layer, high-order nonlinearity/dispersion and absorption, the spatio-temporal evolution of Kerr solitons in the hybrid waveguide leads to a strong self-induced spectral blueshift  $\Delta\lambda \simeq 250 \text{ nm}$ , see Fig. 2(a), as a result of acceleration dynamics in the time-domain, see Fig. 2(b), over a propagation distance of 4 cm. The main limiting factor to obtain larger spectral modulation is represented by

graphene absorption, which quenches the pulse propagation and limits frequency conversion efficiency. However, for higher-order solitons with increased power, graphene absorption becomes saturated as a consequence of partial Pauli-blocking produced by the photo-excited FCs, and the self-induced spectral blue-shift increases, see Fig. 2(c) for soliton order  $N = 2$ . Note in Fig. 2(c) that, thanks to absorption saturation, the self-induced spectral blueshift becomes as large as  $\Delta\lambda \simeq 600$  nm, thus enabling a large spectral tunability of the propagating pulse.

To understand the underlying physics behind FC-induced spectral modulation, in Fig. 3 we plot the normalized FC-density (a)  $\Phi_{\text{FC}}(0, t/t_0)$  at the waveguide input and (d)  $\Phi_{\text{FC}}(z/L_{\text{D}}, t/t_0)$  as a function of the propagation distance  $z$  when the waveguide is excited by a fundamental Kerr soliton ( $N = 1$ ), whose intensity profile  $|\psi(0, t/t_0)|^2 = \text{sech}^2(t/t_0)$  is indicated by the blue line in Fig. 3(a). Owing to the asymmetric temporal profile of  $\Phi_{\text{FC}}(z/L_{\text{D}}, t/t_0)$ , the leading and trailing edges of the pulse experience different FC-induced modulation, which produces temporal acceleration of the input soliton accompanied by a self-induced frequency blue-shift. We evaluate the effect of FC-induced modulation by calculating the correction to the refractive index

$$\Delta n(z/L_{\text{D}}, t/t_0) = \sqrt{\epsilon_{\text{L}} + \epsilon_{\text{NL}}} - \sqrt{\epsilon_{\text{L}}}, \quad (16)$$

where  $\epsilon_{\text{L}} = 1 + i\sigma_0/(\omega_0 \epsilon_0 t_{\text{gr}})$  with  $t_{\text{gr}} (= 0.3 \text{ nm})$  being the thickness of the monolayer graphene and

$$\begin{aligned} \epsilon_{\text{NL}} = & \frac{2c}{\omega_0 L_{\text{D}}} \left[ N^2 (1 + i\tau_{sh} \partial_{\tau}) |\psi|^2 \right. \\ & - d_{\text{FC}} \Phi_{\text{FC}} + i\alpha_0 / \sqrt{1 + 3|\psi|^2/\psi_{\text{sat}}^2} \\ & \left. + \alpha_0 \left( 1 - e^{-\eta_1 \sqrt{3|\psi|^2/\psi_{\text{sat}}^2}} \right) / \sqrt{1 + \eta_2 (3|\psi|^2/\psi_{\text{sat}}^2)^{0.4}} \right] \end{aligned}$$

are the linear and nonlinear dielectric constants, respectively, whose real and imaginary parts at the input ( $z = 0$ ) (b) and output ( $z = 4\text{cm}$ ) (c) are illustrated in Figs. 3(b-c). The spatio-temporal dynamics of the real (e) and imaginary (f) parts of the modulated refractive index  $\Delta n$  are shown in Figs. 3(e-f). Such a time-dependent and asymmetric (solely due to the graphene FCs) refractive index modulation is the inherent ingredient producing a time-dependent phase shift leading to the strong spectral modulation illustrated in Fig. 2.

In order to shed further light on pulse propagation dynamics, we develop a variational treatment where we recast Eq. (14) (after neglecting higher-order terms) in the form of a perturbed NLSE [46]:  $i\partial_{\xi}\psi + \frac{1}{2}\partial_{\tau}^2\psi + |\psi|^2\psi = i\epsilon(\psi)$ , where

$$\begin{aligned} \epsilon(\psi) = & -id_{\text{FC}}\Phi_{\text{FC}}\psi - \alpha_0\psi / \sqrt{1 + 3|\psi|^2/\psi_{\text{sat}}^2} + \quad (17) \\ & + i\alpha_0\psi \left( 1 - e^{-\eta_1 \sqrt{3|\psi|^2/\psi_{\text{sat}}^2}} \right) / \sqrt{1 + \eta_2 (3|\psi|^2/\psi_{\text{sat}}^2)^{0.4}}. \end{aligned}$$

A Lagrangian density  $\mathcal{L}_{\text{D}}$  for such a system can be defined as  $\mathcal{L}_{\text{D}} = (i/2)(\psi^* \partial_{\xi}\psi - \psi \partial_{\xi}\psi^*) + (1/2)(|\psi|^4 - |\partial_{\tau}\psi|^2) -$

$2\text{Re}[i\epsilon\psi^*]$ . The total Lagrangian  $L$  is calculated from the Lagrangian density as  $L = \int_{-\infty}^{\infty} \mathcal{L}_{\text{D}} d\tau$ . Adopting the Ansatz  $\psi = \sqrt{E\eta/2}\mathcal{F}(\tau)e^{i\phi-i\Omega_p(\tau-t_p)-i\beta(\tau-t_p)^2}$ , where  $\mathcal{F}(\tau) = \text{sech}[\eta(\tau - t_p)]$  and the six dimensionless parameters - energy  $E$ , pulse width  $t_{\text{w}} = 2/\eta$ , temporal position  $t_p$ , phase  $\phi$ , frequency shift  $\Omega_p$ , and chirp  $\beta$  become adiabatically evolving functions of the propagation distance  $\xi$ . The Ritz optimization procedure [58] for  $L$  leads to a set of coupled ordinary differential equations (ODEs) describing the evolution of individual pulse parameters

$$\frac{dE}{d\xi} = -2\alpha_0 E \mathcal{K} \text{ atan}(1/\mathcal{K}), \quad (18a)$$

$$\frac{dt_p}{d\xi} = -\Omega_p, \quad (18b)$$

$$\begin{aligned} \frac{d\Omega_p}{d\xi} = & d_{\text{FC}}\Theta_{\text{FC}}(E\eta^3/2) \int_{-\infty}^{\infty} d\tau e^{-\tau/\tau_{\text{FC}}} \times \quad (18c) \\ & \times \mathcal{S}(\tau)\mathcal{F}^2(\tau) \int_{-\infty}^{\tau} \frac{\mathcal{F}^2(\tau')e^{\tau'/\tau_{\text{FC}}}}{\sqrt{1 + \mathcal{F}^2(\tau')/\mathcal{K}^2}} d\tau', \end{aligned}$$

$$\begin{aligned} \frac{d\eta}{d\xi} = & -\alpha_0\eta\mathcal{K} \text{ atan}(1/\mathcal{K}) + 2\beta\eta + \quad (18d) \\ & + (6/\pi^2)\alpha_0\eta^4 \int_{-\infty}^{\infty} \frac{(\tau - t_p)^2\mathcal{F}^2(\tau)}{\sqrt{1 + \mathcal{F}^2(\tau)/\mathcal{K}^2}} d\tau, \end{aligned}$$

$$\begin{aligned} \frac{d\beta}{d\xi} = & 2\beta^2 + \frac{1}{\pi^2}(E\eta^3 - 2\eta^4) + \int_{-\infty}^{\infty} d\tau \mathcal{F}^2(\tau)[1 - 2\mathcal{P}(\tau)] \times \\ & \times \frac{3}{2\pi^2} \left\{ 2\alpha_0\eta^3 \frac{1 - e^{-\eta_1\mathcal{F}(\tau)/\mathcal{K}}}{\sqrt{1 + \eta_2\mathcal{F}^{0.8}(\tau)/\mathcal{K}^{0.8}}} + \right. \quad (18e) \\ & \left. - d_{\text{FC}}\Theta_{\text{FC}}E\eta^4 e^{-\tau/\tau_{\text{FC}}} \int_{-\infty}^{\tau} \frac{\mathcal{F}^2(\tau')e^{\tau'/\tau_{\text{FC}}}}{\sqrt{1 + \mathcal{F}^2(\tau')/\mathcal{K}^2}} d\tau' \right\}, \end{aligned}$$

where  $\mathcal{K} = \sqrt{2\psi_{\text{sat}}^2/3E\eta}$ ,  $\mathcal{S}(\tau) = \tanh[\eta(\tau - t_p)]$  and  $\mathcal{P}(\tau) = \eta(\tau - t_p)\mathcal{S}(\tau)$ .

This set of coupled ODEs provides significant physical insight on the role played by photo-excited FCs because they indicate how perturbations affect the individual pulse parameters. Note, in particular, that photo-excited FCs in graphene directly affect the soliton carrier frequency  $\Omega_p$  because normalized FC generation rate  $\Theta_{\text{FC}}$  appears on the right hand side of Eq. (18d) with an overall positive sign. This immediately implies that soliton dynamics in the hybrid waveguide system drifts towards lower central wavelength accompanied by a temporal acceleration that can be directly inferred from Eq. (18b). The FC-generation induced absorption  $\alpha_0$  enters Eq. (18a) for the soliton energy  $E$ , producing energy quenching. The dynamics of the soliton temporal width  $t_{\text{w}}$  and chirp  $\beta$  is more involved and can be grasped only through numerical integration. We emphasize that the equation for phase  $\phi$  is overlooked here because it does not affect any other soliton parameter. In order to validate the variational predictions, in Fig. 4 we compare the results from the variational approach (blue curves) with data from full numerical simulation of Eqs. (14,15) by the split-step Fast Fourier Transform algorithm com-

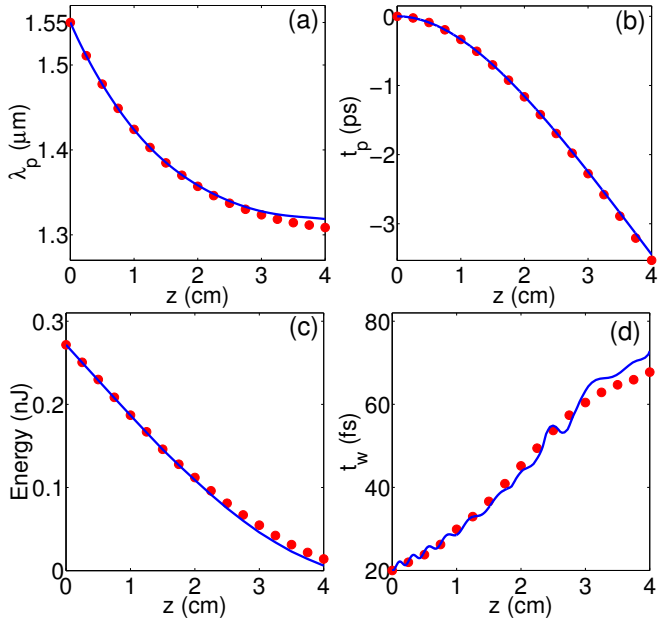


FIG. 4. (Color online) Evolution over the longitudinal coordinate  $z$  of (a) pulse central wavelength  $\lambda_p = 2\pi c/(\omega_0 + \Omega_p/t_0)$ , (b) temporal position  $t_p$ , (c) pulse energy  $E$  and (d) pulse width  $t_w$  of the perturbed Kerr soliton for  $N = 1$ . The solid blue lines indicate predictions from the variational approach through the solution of the coupled ODEs, whereas red circles represent numerical data obtained from the full numerical integration of Eqs. (14,15) by the split-step Fast Fourier Transform algorithm complemented with fourth-order Runge Kutta (neglecting the higher-order terms).

plemented with fourth-order Runge Kutta for the fundamental soliton,  $N = 1$  (solid dots). The set of coupled ODEs [Eqs. (18a)-(18e)] is solved by numerical integration considering input pulse parameters as initial conditions. We find that results from the variational approach are in excellent agreement with direct numerical simulations of Eqs.(14,15). Both approaches indicate a strong central frequency blue-shift up to  $\Delta\lambda \simeq 250$  nm for the fundamental soliton as a consequence of FC generation

is the graphene layer, see Fig. 4(a), and temporal acceleration, see Fig. 4(b). We finally note that the dissipative radiation dynamics ensuing from FC-generation produces quenching of the pulse energy, see Fig. 4(c), and a broadening of the pulse width, see Fig. 4(d). However, as discussed above, absorption can be saturated by higher energy pulses thanks to partial Pauli-blocking of the photo-induced FCs, see Fig. 2, leading to self-induced spectral blueshift as large as  $\Delta\lambda \simeq 600$  nm.

#### IV. CONCLUSIONS

We have developed from first principles a theoretical model enabling the description of infrared pulse propagation in graphene-covered hybrid waveguides. Our theoretical model finely accounts for the waveguide dispersion, the nonlinearity of the waveguide core, and the effect produced by photo-generated FCs in the graphene layer. Specializing our calculations to a realistic rectangular waveguide composed of TaFD5 glass on top of silica substrate and covered with graphene on top, we find that FC generation enables efficient spectral modulation of ultrafast pulses propagating in the waveguide. In particular, we observe a strong spectral blue-shift of several hundreds of nanometers for peak pulse powers of the order of 10 kW. We further validate numerical results with a variational approach indicating that the refractive index temporal modulation ensuing from FC generation is responsible for the observed spectral modulation. Our results indicate that graphene-covered hybrid waveguides offer an appealing platform for frequency conversion in integrated optoelectronic devices.

#### ACKNOWLEDGMENTS

S.R. acknowledges funding from Shri Gopal Rajgarhia International Programme-Indian Institute of Technology (SGRIP-IIT) Kharagpur for the collaborative visit of A.M.

---

[1] A. E. Willner, S. Khaleghi, M. R. Chitgarha, and O. F. Yilmaz, *J. Light. Technol.* **32**, 660 - 680 (2014).

[2] J. Schoetz, Z. Wang, E. Pisanty, M. Lewenstein, M. F. Kling, and M. F. Ciappina, *ACS Photonics* **6**, 3057 - 3069 (2019).

[3] S. M. Hendrickson, A. C. Foster, R. M. Camacho, and B. D. Clader, *J. Opt. Soc. Am. B* **31**, 3193 - 3203 (2014).

[4] D. Thomson, A. Zilkie, J. E. Bowers, T. Komljenovic, G. T. Reed, L. Vivien, D. Marris-Morini, E. Cassan, L. Virot, J.-M. Fedeli, J.-M. Hartmann, J. H. Schmid, D.-X. Xu, F. Boeuf, P. O'Brien, G. Z. Mashanovich., and M. Nedeljkovic, **18**, 073003 (2016).

[5] V. Mizrahi, K. W. DeLong, G. I. Stegeman, M. A. Saifi, and M. J. Andrejco, *Opt. Lett.* **14**, 1140 - 1142 (1989).

[6] H. K. Tsang, C. S. Wong, T. K. Liang, I. E. Day, S. W. Roberts, A. Harpin, J. Drake, and M. Asghari, *Appl. Phys. Lett.* **80**, 416 - 418 (2002).

[7] C. Koos, L. Jacome, C. Poulton, J. Leuthold, and W. Freude, *Opt. Express* **15**, 5976 - 5990 (2007).

[8] E. Ozbay, *Science* **311**, 189 - 193 (2006).

[9] A. Tuniz, O. Bickerton, F. J. Diaz, T. Kasebier, E.-B. Kley, S. Kroker, S. Palomba, and C. M. de Sterke, *Nat. Commun.* **11**, 2413 (2020).

[10] N. Rotenberg, A. Bristow, M. Pfeiffer, M. Betz, and H. Van Driel, *Phys. Rev. B* **75**, 155426 (2007).

- [11] M. Scalora, M. A. Vincenti, D. de Ceglia, V. Roppo, M. Centini, N. Akozbek, and M. J. Bloemer, *Phys. Rev. A* **82**, 043828 (2010).
- [12] P. Ginzburg, A. Hayat, N. Berkovitch, and M. Orenstein, *Opt. Lett.* **35**, 1551 - 1553 (2010).
- [13] A. Marini, M. Conforti, G. Della Valle, H. W. Lee, Tr. X. Tran, W. Chang, M. A. Schmidt, S. Longhi, P. St.J. Russell, and F. Biancalana, *New J. Phys.* **15**, 013033 (2013).
- [14] I. De Leon, Z. Shi, A. C. Liapis, and R. W. Boyd, *Opt. Letters* **39**, 2274 - 2277 (2014).
- [15] A. Tuniz, S. Palomba, C. M. de Sterke, *Appl. Phys. Lett.* **117**, 071105 (2020)
- [16] A. Marini, R. Hartley, A. V. Gorbach, and D. V. Skryabin, *Phys. Rev. A* **84**, 063839 (2011).
- [17] D. V. Skryabin, A. V. Gorbach, and A. Marini, *J. Opt. Soc. Am. B* **28**, 109 - 114 (2011).
- [18] G. Li, C. M. de Sterke, and S. Palomba, *Opt. Lett.* **42**, 1329 - 1332 (2017).
- [19] J. B. Khurgin, *Nat. Nanotechnol.* **10**, 2 - 6 (2015).
- [20] D. J. Bergman and M. I. Stockman, *Phys. Rev. Lett.* **90**, 027402 (2003).
- [21] M. A. Noginov, G. Zhu, A. M. Belgrave, R. Bakker, V. M. Shalaev, E. E. Narimanov, S. Stout, E. Herz, T. Suteewong, and U. Wiesner, *Nature* **460**, 1110 - 1113 (2009).
- [22] A. Marini, A. V. Gorbach, D. V. Skryabin, and A. V. Zayats, *Opt. Lett.* **34**, 2864 - 2866 (2009).
- [23] M. I. Stockman, *J. Opt.* **12**, 024004 (2010).
- [24] I. De Leon and P. Berini, *Nat. Photonics* **4**, 382 - 387 (2010).
- [25] J. Y. Suh, C. H. Kim, W. Zhou, M. D. Huntington, D. T. Co, M. R. Wasielewski, and T. W. Odom, *Nano Lett.* **12**, 5769 - 5774 (2012).
- [26] A. Yang, T. B. Hoang, M. Dridi, C. Deeb, M. H. Mikkelsen, G. C. Schatz, and T. W. Odom, *Nat. Commun.* **6**, 6939 (2015).
- [27] Y. Wu, C. Zhang, N. M. Estakhri, Y. Zhao, J. Kim, M. Zhang, X. Liu, G. K. Pribil, A. Alu, C. Shih, and X. Li, *Adv. Mater.* **26**, 6106 - 6110 (2014).
- [28] A. Marini and F. Biancalana, *Phys. Rev. Lett.* **110**, 243901 (2013).
- [29] F. Bonaccorso, Z. Sun, T. Hasan, and A. C. Ferrari, *Nat. Photonics* **4**, 611 - 622 (2010).
- [30] K. S. Novoselov, A. K. Geim, S. V. Morozov, D. Jiang, M. I. Katsnelson, I. V. Grigorieva, S. V. Dubonos, and A. A. Firsov, *Nature* **438**, 197 (2005).
- [31] L. Wang et al., *Science* **342**, 614 - 617 (2013).
- [32] A. H. Castro Neto, F. Guinea, N. M. R. Peres, K. S. Novoselov, and A. K. Geim, *Rev. Mod. Phys.* **81**, 109 (2009).
- [33] S. A. Mikhailov and K. Ziegler, *J. Phys.: Condens. Matter* **20**, 384204 (2008).
- [34] A. R. Wright, X. G. Xu, J. C. Cao, and C. Zhang, *Appl. Phys. Lett.* **95**, 072101 (2009).
- [35] K. L. Ishikawa, *Phys. Rev. B* **82**, 201402(R) (2010).
- [36] E. Hendry, P. J. Hale, J. Moger, A. K. Savchenko, and S. A. Mikhailov, *Phys. Rev. Lett.* **105**, 097401 (2010).
- [37] R. Wu et al., *Nano Lett.* **11**, 5159 - 5164 (2011).
- [38] J. L. Cheng, N. Vermeulen, and J. E. Sipe, *New J. Phys.* **16**, 053014 (2014).
- [39] P. Bowlan, E. Martinez-Moreno, K. Reimann, T. Elsaesser, and M. Woerner, *Phys. Rev. B* **89**, 041408(R) (2014).
- [40] J. D. Cox, A. Marini, and F. J. García de Abajo, *Nat. Commun.* **8**, 14380 (2017).
- [41] J. D. Cox and F. J. García de Abajo, *Acc. Chem. Res.* **52**, 2536 - 2547 (2019).
- [42] M. Baudisch, A. Marini, J. D. Cox, T. Zhu, F. Silva, S. Teichmann, M. Massicotte, F. Koppens, L. S. Levitov, F. J. García de Abajo, and J. Biegert, *Nat. Commun.* **9**, 1018 (2018).
- [43] N. Vermeulen et al., *Nat. Commun.* **9**, 2675 (2018).
- [44] D. Castelló-Lurbe, H. Thienpont, and N. Vermeulen, *Laser Photonics Rev.* **14**, 1900402 (2020).
- [45] A. Bondeson, M. Lisak, and D. Anderson, *Phys. Scr.* **20**, 479 (1979).
- [46] G. P. Agrawal, *Nonlinear Fiber Optics*, 5th ed. (Academic Press, New York, 2013).
- [47] A. Marini, J. D. Cox, and F. J. García de Abajo, *Phys. Rev. B* **95**, 125408 (2017).
- [48] S. Franzen, *J. Phys. Chem. C* **112**, 6027 - 6032 (2008).
- [49] X. Liu, J. Park, J. Kang, H. Yuan, Y. Cui, H. Y. Hwang, and M. L. Brongersma, *Appl. Phys. Lett.* **105**, 181117 (2014).
- [50] O. Fedotova, A. Husakou, and J. Herrmann, *Opt. Exp.* **14**, 1512 (2006).
- [51] I. Babushkin, A. Husakou, J. Herrmann, and Yuri S. Kivshar, *Opt. Exp.* **15**, 11978 (2007).
- [52] D. N. Christodoulides, I. C. Khoo, G. J. Salamo, G. I. Stegeman and E. W. Van Stryland *Adv. Opt. Photon.* **2**, 60 (2010).
- [53] H. Guo, C. Herkommer, A. Billat, et al., *Nat. Photon.* **12**, 330-335 (2018).
- [54] Finite-element frequency domain calculations of the plasmonic waveguide dispersion, field distributions, and nonlinear coefficients have been carried out using COMSOL Multiphysics® v. 4.4. [www.comsol.com](http://www.comsol.com), COMSOL AB, Stockholm, Sweden.
- [55] A. Marini and F. J. García de Abajo, *Phys. Rev. Lett.* **116**, 217401 (2016).
- [56] A. V. Gorbach, A. Marini, and D. V. Skryabin, *Opt. Lett.* **38**, 5244-5247 (2013).
- [57] D. V. Skryabin, F. Luan, J. C. Knight, and P. St. J. Russell, *Science* **301**, 1705-1708 (2003).
- [58] D. Anderson *Phys. Rev. A* **27**, 3135 (1983).